

# Redshift Evolution and Non-Universal Dispersion of Quasar Luminosity Correlation

Zhuoyang Li, Lu Huang<sup>\*</sup>, Junchao Wang

<sup>1</sup>*School of Physics and Astronomy, Sun Yat-Sen University, 2 Daxue Road, Tangjia, Zhuhai, 519082, P.R.China*

Accepted 2022 September 22. Received 2022 August 22; in original form 2022 May 24

## ABSTRACT

The standard  $\Lambda$ CDM model is recently reported to deviate from the high-redshift Hubble diagram of type Ia supernovae (SNe) and quasars (QSOs) at  $\sim 4\sigma$  confidence level. In this work, we combine the PAge approximation (a nearly model-independent parameterization) and a high-quality QSO sample to search for the origins of the deviation. By visualizing the  $\Lambda$ CDM model and the marginalized  $3\sigma$  constraints of SNe+QSOs into PAge space, we confirm that the SNe+QSOs constraints in both flat and non-flat PAge cases are in remarkable tension with the standard  $\Lambda$ CDM cosmology. Next, we investigate the tension from the perspective of redshift-evolution effects. We find that the QSO correlation coefficient  $\gamma$  calibrated by SNe+low- $z$  QSOs and SNe+high- $z$  QSOs shows  $\sim 2.7\sigma$  and  $\sim 4\sigma$  tensions in flat and non-flat universes, respectively. The tensions for intrinsic dispersion  $\delta$  between different data sets are found to be  $> 4\sigma$  in both flat and non-flat cases. These results indicate that the QSO luminosity correlation suffers from significant redshift evolution and non-universal intrinsic dispersion. Using a redshift-dependence correlation to build QSO Hubble diagram could lead to biases. Thus, the  $\sim 4\sigma$  deviation from the standard  $\Lambda$ CDM probably originates from the redshift-evolution effects and non-universal dispersion of the QSO luminosity correlation rather than new physics.

**Key words:** quasars: general – cosmological parameters – dark energy – observations

## 1 INTRODUCTION

The phenomenon of cosmic accelerating expansion is firstly indicated by observing the extra dimming of the high-redshift Type Ia supernovae (SNe) (Perlmutter et al. 1997; Riess et al. 1998; Schmidt et al. 1998; Perlmutter et al. 1999). A widely accepted explanation of this mysterious phenomenon is that a hypothetical dark energy component with negative pressure drives the homogeneous and isotropic universe to accelerate. Interpreting dark energy as a cosmological constant  $\Lambda$  and assuming the validity of general relativity at all scales and epochs, the standard  $\Lambda$  cold dark matter ( $\Lambda$ CDM) model has achieved remarkable success in agreeing with a great majority of cosmological observational measurements (Scolnic et al. 2018; Alam et al. 2021; Jimenez & Loeb 2002; Abbott et al. 2022; Aghanim et al. 2020). However, these modern cosmological measurements are restricted to either the low redshift range ( $0 \leq z \leq 2.33$ ) or the high redshift range ( $z \sim 1100$ ). The cosmic expansion history is still poorly explored in the redshift interval ( $2.33 < z < 1100$ ) which is very essential for studying the dark energy models beyond the typical  $\Lambda$ CDM physic.

As the most luminous and persistent energy sources in our Universe, quasars (QSOs) serve as a potential candidate for high-redshift cosmological tests which can be detected up to redshift  $\sim 7.64$  (Yang et al. 2021; Wang et al. 2021). Several empirical correlations between spectral features and luminosity have been proposed to enable QSOs

as competitive cosmological tools (Baldwin 1977; Watson et al. 2011; La Franca et al. 2014; Wang et al. 2014). Particularly, the most investigated and best constructed QSO luminosity correlation is the observed non-linear correlation between ultraviolet ( $L_{UV}$  at 2500Å) and X-ray ( $L_X$  at 2 keV) luminosity which is firstly proposed in Tananbaum et al. (1979); Griffiths et al. (1981); Tananbaum et al. (1986) and subsequently developed in (Risaliti & Lusso 2015; Lusso & Risaliti 2016, 2017; Risaliti & Lusso 2019; Lusso 2019; Salvestrini et al. 2019; Lusso et al. 2020; Bisogni et al. 2021). Although the detailed physical mechanism of the  $L_{UV} - L_X$  correlation still remains unknown (Haardt & Maraschi 1991, 1993; Ghisellini & Haardt 1994; Nicastro 2000; Merloni 2003; Arcodia et al. 2019), the authors in Lusso et al. (2020) have minimized all of the possibles systematic effects and proven the stability of this QSO luminosity correlation. Based on the  $L_{UV} - L_X$  correlation, Risaliti & Lusso (2019) utilized a new technique to model-independently build the QSO Hubble diagram and extend it to  $z \sim 5.5$ . A good agreement is found between the constructed QSO Hubble diagram and the  $\Lambda$ CDM model at  $z < 1.4$  while a  $\sim 4\sigma$  deviation emerges at higher redshift range. Two follow-up works further confirm this significant deviation with more precise approaches and cleaner QSO samples (Lusso et al. 2019, 2020). Since then, the deviation between the high-redshift QSOs Hubble diagram and the  $\Lambda$ CDM model arises heated debates (Melia 2019; Yang et al. 2020; Velten & Gomes 2020; Mehrabi & Basilakos 2020; Zheng et al. 2021; Lian et al. 2021; Colgáin et al. 2022; Li et al. 2021; Khadka & Ratra 2021, 2022).

Velten & Gomes (2020) used a model-independent estimator to

\* E-mail: huanglu37@mail2.sysu.edu.cn

test the robustness of the QSO Hubble diagram. Their result suggests that the QSO data can not be used as a reliable cosmological tool because it even fails to state the cosmic accelerating expansion phase. [Yang et al. \(2020\)](#) claimed that the model-independent approach developed in [Risaliti & Lusso \(2019\)](#) failed to recover the high- $z$  cosmic expansion history of the flat  $\Lambda$ CDM model, which undermined the  $\sim 4\sigma$  deviation. Using the Gaussian process and a combination of SNIa, Quasars and gamma-ray burst data, [Mehrabi & Basilakos \(2020\)](#) found a less significant tension. They argued that the amount of the deviation might be affected by the choice of the kernel function. All these works challenge the claimed  $\sim 4\sigma$  deviation. However, the main cause of the deviation is still not found.

Our aim in this present work is to search for the possible origins of the significant deviation between the  $\Lambda$ CDM model and the high- $z$  Hubble diagram of SNe+QSOs. The key is to adopt model-independent approaches and independent samples. To avoid model dependence, we perform our analyses in PAge approximation (Parameterization based on cosmic Age) which is a general approximation of many late-time cosmological models and a nearly model-independent framework ([Huang 2020; Luo et al. 2020; Huang et al. 2021b,a, 2022; Cai et al. 2022a,b; Huang 2022](#)). In addition, we take the most up-to-date QSO samples compiled by [Lusso et al. \(2020\)](#) as our data set.

Our work is organized as follows. We present the advantages of the PAge approximation in the next Section 2. The data and methodology are briefly introduced in Section 3. The detailed results are shown in Section 4. In the last Section 5, we conclude and discuss.

## 2 COSMOLOGICAL SCENE

The logarithm polynomial parameterization was firstly proposed to quantify the deviation between the concordance  $\Lambda$ CDM cosmology and the high- $z$  QSO Hubble diagram in [Risaliti & Lusso \(2019\)](#). It defines the luminosity distance with a polynomial function of  $\log_{10}(1+z)$

$$d_L(z) = \frac{c \ln(10)}{H_0} \sum_{i=1}^n a_i \log_{10}^i(1+z), \quad (1)$$

where  $a_i$  are free parameters, except  $a_1 = 1$ .  $c$  is the speed of light.  $H_0$  is the Hubble constant.

Based on the Taylor expansion in  $\log_{10}(1+z)$ , this parameterization provides a model-independent exploration of the late-time cosmological expansion history and approximates many cosmological models accurately at low redshift ( $z \lesssim 1$ ). However, its approximation precision worsens considerably when  $z$  exceeds 1, as shown in Table 1 (here we take its 4th-order expansion as an example). For the redshift range  $[0, 8]$ , the maximum relative errors in luminosity distance are more than 2% for different  $\Lambda$ CDM models, which may cause biases in data fitting. Introducing higher orders in  $\log_{10}(1+z)$  could certainly improve the fitting precision but also weaken the constraint power of data and complicate the procedure of comparing with the standard  $\Lambda$ CDM model.

Compared to the logarithm polynomial approximation, the recently proposed PAge approximation displays many prominent advantages in blindly modelling the late cosmological expansion history ([Huang 2020; Luo et al. 2020; Huang et al. 2021b,a, 2022; Cai et al. 2022a,b; Huang 2022](#)). Faithfully obeying the asymptotic matter-dominated assumption  $\frac{1}{1+z} \propto t^{\frac{2}{3}}$  at high redshift  $z \gg 1$  (the radiation component is not taken into consideration), PAge models the Hubble

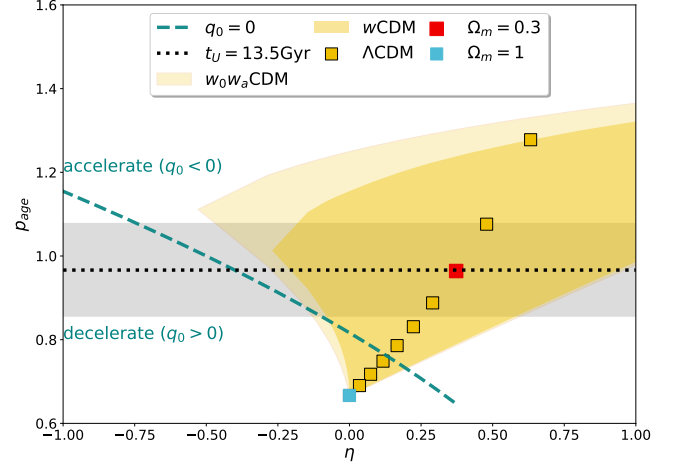


**Figure 1.** Mapping the  $\Lambda$ CDM,  $w$ CDM and  $w_0-w_\alpha$ CDM models into  $(p_{\text{age}}, \eta)$  plane. We map the cosmological models into  $(p_{\text{age}}, \eta)$  plane by matching the deceleration parameter  $q_0$  at  $z=0$  ([Luo et al. 2020](#)). The  $\Lambda$ CDM models are mapped into a sequence of discrete points ( $\Omega_m \in [0.1, 1]$  with step length 0.1). The  $w$ CDM models ( $\Omega_m \in [0.1, 1]$ ,  $w \in [-1.5, -0.5]$ ) and  $w_0-w_\alpha$ CDM models ( $\Omega_m \in [0.1, 1]$ ,  $w_0 \in [-1.5, -0.5]$ ,  $w_\alpha \in [0.5, 1.5]$ ) are mapped into yellow areas. The green dashed line divides the  $(p_{\text{age}}, \eta)$  plane into cosmic deceleration and acceleration regions. The black dotted line and grey region represent the cosmic age and its  $3\sigma$  bound inferred in [Valcin et al. \(2020\)](#). The red point and blue point are the standard  $\Lambda$ CDM and CDM models.

expansion rate as a function of cosmological time  $t$ ,

$$\frac{H}{H_0} = 1 + \frac{2}{3} \left(1 - \eta \frac{H_0 t}{p_{\text{age}}}\right) \left(\frac{1}{H_0 t} - \frac{1}{p_{\text{age}}}\right), \quad (2)$$

where the dimensionless parameter  $p_{\text{age}} \equiv H_0 t_0$  measures the cosmic age  $t_0$  (both  $t$  and  $t_0$  are in unit of  $H_0^{-1}$ ), and the dimensionless parameter  $\eta$  characterizes the deviation from Einstein de-sitter universe (flat CDM model). We set a bound condition  $\eta < 1$  to guarantee the fundamental physical features, e.g.  $\frac{dL}{dz} > 0$  and  $\frac{dH}{dz} > 0$  ([Huang 2020](#)).

Doing cosmological tests with PAge approximation has some distinct advantages, as follows:

1) The cosmic age  $t_0$  absorbed in  $p_{\text{age}}$  parameter is easily applied to do astronomical tests ([Luo et al. 2020](#)). More specifically, [Valcin et al. \(2020\)](#) presented an independent inference of  $t_0 = 13.5^{+0.16}_{-0.14}$  (stat.)  $\pm 0.5$  (sys.) from the full colour-magnitude diagram of the globular cluster. If a cosmological model predicts a significantly different  $t_0$  compared to the above estimation, it can be ruled out safely. For instance, the flat CDM model corresponding to  $p_{\text{age}} = \frac{2}{3}$ ,  $\eta = 0$  in PAge approximation fails to accommodate this cosmic age inference, which is clearly shown in Figure 1.

2) The cosmic deceleration and acceleration are easy to distinguish in PAge. According to  $\eta = 1 - \frac{3}{2} p_{\text{age}}^2 (1 + q_0)$  ([Luo et al. 2020](#)), the PAge universe is divided into decelerating and accelerating regions in Figure 1.

3) As an almost model-independent framework, PAge is able to precisely approximate a broad class of physical models by matching the deceleration parameter  $q_0$  or by doing a least-square fitting of cosmological observables (see [Huang 2020; Luo et al. 2020; Huang et al. 2021b,a](#)). The maximum relative errors of luminosity distance

**Table 1.** Comparisons of maximum relative errors in luminosity distance ( $d_L$ ) between 4th-order logarithmic polynomial expansion and PAge approximation.

fiducial cosmology	-	4th-order logarithmic polynomial expansion	PAge approximation
$\Lambda$ CDM	redshift ranges	$\max \frac{\Delta d_L}{d_L} $	$\max \frac{\Delta d_L}{d_L} $
$\Omega_m = 0.3$	[0,1]	$7.33 \times 10^{-5}$	$3.82 \times 10^{-4}$
	[0,2]	$1.74 \times 10^{-3}$	$1.07 \times 10^{-3}$
	[0,4]	$1.04 \times 10^{-2}$	$2.00 \times 10^{-3}$
	[0,8]	$3.72 \times 10^{-2}$	$2.85 \times 10^{-3}$
$\Omega_m = 0.5$	[0,8]	$2.61 \times 10^{-2}$	$9.86 \times 10^{-4}$
$\Omega_m = 0.7$	[0,8]	$2.04 \times 10^{-2}$	$2.68 \times 10^{-4}$

( $d_L$ ) are controlled below 0.3%, and it is well held for both low redshift and high redshift, as indicated in Table 1.

4) Utilizing PAge approximation to do Bayesian analysis is economical, effective, and concise. Generally, many typical physical models can be approximately mapped into the ( $p_{\text{age}}, \eta$ ) plane, and some of them are superimposed onto one point (we visualize this unique feature in Figure 1). Performing data analysis with PAge provides the Bayesian evidence for all the models which are included in the marginalized contour of  $p_{\text{age}}$  and  $\eta$  parameters. This practice avoids the cumbersome and complex process of computing Bayesian evidence for all the models.

Almost having the same advantages as the logarithm polynomial approximation (Yang et al. 2020), PAge merely has two nuisance parameters ( $p_{\text{age}}, \eta$ ) and simultaneously has reliable fitting precision at both low- $z$  and high- $z$ . Since PAge displays many superiorities and can accurately describe the expansion history of the high- $z$  universe, we utilize it to do an independent analysis of QSO cosmology.

### 3 DATA AND METHODOLOGY

A high-quality QSO sample is recently compiled in Lusso et al. (2020). This new sample includes 2421 optically selected QSOs with spectroscopic redshift (span the redshift interval  $0.009 \leq z \leq 7.5413$ ) and X-ray observations. Systematic effects and low-quality measurements are largely removed by applying a couple of preliminary filters. For example, 30% X-ray measurements are excluded by the conditions:  $\Delta F_s/F_s < 1$  and  $\Delta F_H/F_H < 1$ . More detailed filter procedures are discussed in Lusso et al. (2020). After an optimal selection of clean sources, this high-quality QSO sample is suitable for investigating the non-linear relation between the ultraviolet (at 2500 Å,  $L_{\text{UV}}$ ) and X-ray (at 2keV,  $L_X$ ) luminosity of QSO:

$$\log_{10} L_X = \gamma \log_{10} L_{\text{UV}} + \beta, \quad (3)$$

where  $\gamma, \beta$  are free parameters.  $L_X$  and  $L_{\text{UV}}$  are the rest-frame monochromatic luminosities which follow the standard luminosity-flux relation  $L = 4\pi d_L^2 F$ . Further expressing Eq. 3 with flux, one

obtains

$$\log_{10} F_X = \gamma \log_{10} F_{\text{UV}} + (\gamma - 1) \log_{10} (4\pi d_L^2) + \beta, \quad (4)$$

both  $F_X$  and  $F_{\text{UV}}$  are the flux densities in the unit of erg/s/cm<sup>2</sup>. We quantify the uncertainties of  $\gamma, \beta$  and the variability of cosmologies with the joint likelihood function (D'Agostini 2005):

$$\ln \mathcal{L} \propto -\frac{1}{2} \sum_{i=1}^N \left[ \frac{(\log_{10} F_{X,i}^{\text{obs}} - \log_{10} F_{X,i}^{\text{th}})^2}{\sigma_{\text{total}}^2} + \ln(2\pi\sigma_{\text{total}}^2) \right], \quad (5)$$

the total uncertainties  $\sigma_{\text{total}}^2 = \sigma_{F_{X,i}^{\text{obs}}}^2 + \gamma^2 \sigma_{F_{\text{UV},i}^{\text{obs}}}^2 + \delta^2$ , where  $\delta$  is a scatter parameter representing uncounted extra variability.

It is worth noting that the QSOs can not be used to do cosmological tests directly because they do not provide absolute distance values (Bargiacchi et al. 2022). A cross-calibration procedure is needed to match the distance values between QSOs and SNe in the common redshift range. The detailed calibration procedure is to multiply the luminosity distance by a calibration parameter  $k$ , i.e.  $d_L^{\text{calibration}}(z) = k d_L^{\text{model}}(z)$ , and the  $k$  parameter requires a simultaneous fitting of QSOs and SNe. In the cross-calibration procedure,  $k$  degenerates with  $H_0$ . To avoid parameter degeneracy, we fix  $H_0 = 70$  km/s/Mpc in the following analyses. We calibrate the QSO distances with the Pantheon SNe sample (Scolnic et al. 2018) and use the combination data set of SNe+QSOs to build the QSO Hubble diagram.

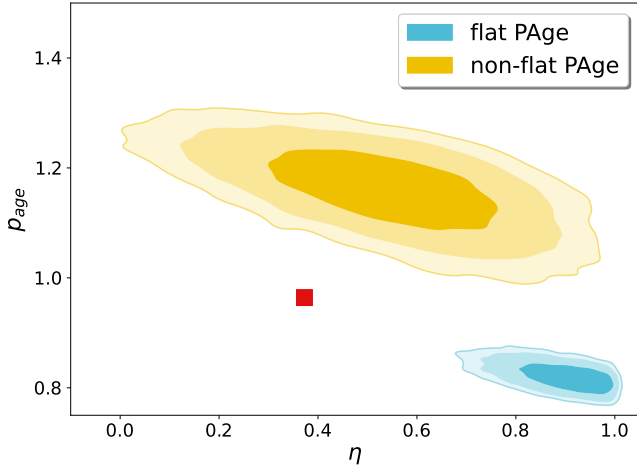
As indicated in Table 2 of Bargiacchi et al. (2022), the spatial curvature has a great impact on the cosmological constraints when using QSO data. The joint analysis of SNe+QSO in non-flat  $\Lambda$ CDM background prefers a closed universe with spatial curvature  $\Omega_k \simeq -0.6$ , which is inconsistent with the Planck+CMB result  $\Omega_k = -0.044^{+0.018}_{-0.015}$  (Aghanim et al. 2020). To not miss some important information, we consider both flat and non-flat cosmological cases in the following analyses.

### 4 RESULTS

In Table 2, we list the marginalized  $1\sigma$  constraints on parameters with SNe+QSOs data in PAge backgrounds. Both the flat and non-

**Table 2.** Marginalized  $1\sigma$  constraints on parameters with SNe+QSOs samples in PAge backgrounds.

model	$\Omega_k$	$p_{\text{age}}$	$\eta$	$\gamma$	$\beta$	$\delta$
flat PAge	-	$0.820^{+0.017}_{-0.02}$	$0.896^{+0.089}_{-0.038}$	$0.642 \pm 0.0083$	$6.96^{+0.33}_{-0.29}$	$0.228 \pm 0.0034$
non-flat PAge	$-0.946^{+0.017}_{-0.051}$	$1.16 \pm 0.051$	$0.540^{+0.17}_{-0.14}$	$0.619 \pm 0.009$	$7.68 \pm 0.33$	$0.226 \pm 0.0036$

**Figure 2.** Marginalized  $1\sigma$ ,  $2\sigma$  and  $3\sigma$  constraints on PAge parameters with SNe+QSOs samples. Both flat and non-flat PAge universes are taken into account. The red point represents the standard  $\Lambda$ CDM which corresponds to the point ( $p_{\text{age}} = 0.964$ ,  $\eta = 0.373$ ) in PAge panel.

flat cases are taken into consideration. For better comparison with the standard  $\Lambda$ CDM model, we visualize the marginalized  $1\sigma$ ,  $2\sigma$  and  $3\sigma$  constraints on PAge parameters in Figure 2. We find both the marginalized contours on  $p_{\text{age}}$  and  $\eta$  in flat and non-flat PAge cases significantly deviate from the standard  $\Lambda$ CDM model (red point in Figure 2) at  $> 3\sigma$  confidence level. The marginalized contours of the flat and non-flat PAge cases also show a  $> 3\sigma$  discrepancy, which indicates the inferences of PAge parameters are much affected by the addition of spatial curvature  $\Omega_k$  freedom. Indeed, the spatial curvature  $\Omega_k$  is found to be  $-0.946^{+0.017}_{-0.051}$ , which strongly supports a closed universe. And the exotic  $\Omega_k$  inference is actually inconsistent with other measurements (Scolnic et al. 2018; Alam et al. 2021; Jimenez & Loeb 2002; Abbott et al. 2022; Aghanim et al. 2020).

The SNe+QSOs constraints on PAge parameters in both flat and non-flat universes seem to suggest new physics beyond the  $\Lambda$ CDM. However, whether the QSOs can serve as a reliable cosmological tool still requires cautious research. As mentioned in Lusso et al. (2020), using the non-linear QSO luminosity correlation to build the QSO Hubble diagram may still have shortcomings. For example, the systematics in the QSO samples selection, the process used to fit the QSO Hubble diagram and the redshift evolution effect of QSO luminosity correlation may cause biases and lead to an unreliable QSO Hubble diagram. Possible systematics have been carefully checked in Lusso et al. (2020) and we focus on the redshift evolution effect of the QSO luminosity correlation in this present work.

Different from the narrow redshift bins split in Risaliti & Lusso (2019); Lusso et al. (2020), we divide QSO samples into the low- $z$

( $z \leq 1.5$ ) bin and high- $z$  bin ( $z > 1.5$ ) to test the redshift evolution, because the strong deviation from  $\Lambda$ CDM model roughly emerges at  $z > 1.5$ . We analyze the SNe+low- $z$  QSOs and SNe+high- $z$  QSOs data sets in flat and non-flat PAge backgrounds, respectively. The marginalized  $1\sigma$  constraints on the PAge parameters, QSO correlation coefficients and intrinsic dispersion are presented in Table 3.

Either in flat or in non-flat PAge cases, significant evolutionary trends emerge for the  $\gamma$ ,  $\delta$  parameters. For the  $\gamma$  parameter, we find  $\sim 2.7\sigma$  and  $\sim 4\sigma$  discrepancies between the two data sets in flat and non-flat PAge universes respectively. For the  $\delta$  parameter, the discrepancies are found to be  $> 4\sigma$  in different PAge backgrounds. These results indicate that the QSO luminosity correlation evolves with redshift and suffers from non-universal dispersion. In addition, we find the PAge parameters inferred from the SNe+low- $z$  QSOs and SNe+high- $z$  QSOs data sets, as shown in Figure 3, coincide well. More importantly, the marginalized  $3\sigma$  contour of SNe+high- $z$  QSOs deviates from the  $\Lambda$ CDM significantly while the SNe+low- $z$  QSOs case roughly accommodates it, which implies that the PAge parameter inferences are probably biased by the redshift evolution and non-universal dispersion.

In the Bayesian framework, performing a linear fit between two data sets with errors on both axes and with an extra variance is quite subtle. Different analysis methods may yield inconsistent results, as indicated in Guidorzi et al. (2006). In our above analyses, we use the likelihood function (5) derived by D’Agostini (2005) to estimate the parameters and find remarkable discrepancies for  $\gamma$ ,  $\delta$  parameters. To demonstrate the discrepancies are not dominated by the statistical analysis method, we further perform Bayesian analyses with the Reichart method (Reichart 2001; Reichart et al. 2001) and present the parameter inference results in Table 4.

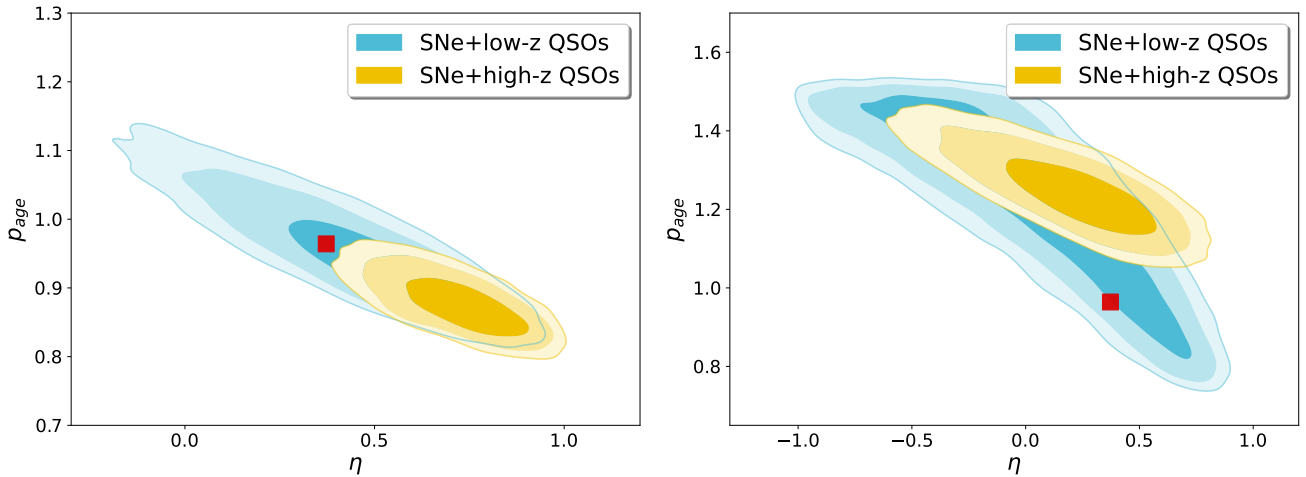
According to Table 4, we find the  $\gamma$ ,  $\delta$  parameters derived from the Reichart method also show prominent discrepancies. The  $\gamma$  parameters calibrated by SNe+low- $z$  QSOs samples are in  $\sim 3.4\sigma$  and  $\sim 4.1\sigma$  tension with that calibrated by SNe+high- $z$  QSOs samples in flat and non-flat PAge respectively. The  $\delta$  parameters show  $\sim 4.0\sigma$  and  $\sim 4.4\sigma$  discrepancies between different data sets and backgrounds. This suggests that the redshift-evolution effect and non-universal dispersion of QSO luminosity correlation are independent of the statistical analysis method.

## 5 CONCLUSIONS AND DISCUSSION

In this research, we provide an independent search for the origins of the  $\sim 4\sigma$  deviation between the standard  $\Lambda$ CDM model and the constructed Hubble diagram of SNe+QSOs (Risaliti & Lusso 2019; Lusso et al. 2019, 2020). We adopt a nearly model-independent parameterization (PAge approximation) to visualize the standard  $\Lambda$ CDM model and marginalized  $3\sigma$  constraints of SNe+QSOs data. To a certain degree, we have avoided the model dependence and

**Table 3.** Marginalized  $1\sigma$  constraints on parameters with SNe+low-z QSOs sample and SNe+high-z QSOs sample respectively.

model	sample	$\Omega_k$	$p_{\text{age}}$	$\eta$	$\gamma$	$\beta$	$\delta$
flat PAge	SNe+low-z QSOs	-	$0.940^{+0.033}_{-0.062}$	$0.480^{+0.21}_{-0.13}$	$0.637 \pm 0.013$	$7.18 \pm 0.41$	$0.237 \pm 0.0047$
	SNe+high-z QSOs	-	$0.875^{+0.025}_{-0.032}$	$0.727^{+0.12}_{-0.096}$	$0.585 \pm 0.014$	$8.80^{+0.52}_{-0.43}$	$0.207 \pm 0.0054$
non-flat PAge	SNe+low-z QSOs	$-0.512^{+0.096}_{-0.35}$	$1.21^{+0.28}_{-0.10}$	$0.05^{+0.48}_{-0.35}$	$0.635 \pm 0.013$	$7.21 \pm 0.43$	$0.237 \pm 0.0047$
	SNe+high-z QSOs	$-0.795 \pm 0.078$	$1.24^{+0.057}_{-0.071}$	$0.220^{+0.26}_{-0.19}$	$0.561^{+0.0088}_{-0.013}$	$9.49^{+0.49}_{-0.15}$	$0.203 \pm 0.0053$

**Figure 3.** Marginalized  $1\sigma$ ,  $2\sigma$  and  $3\sigma$  constraints on PAge parameters with SNe+low-z QSOs and SNe+high-z QSOs samples in flat and non-flat PAge universes, respectively. The red point represents the standard  $\Lambda$ CDM model.**Table 4.** Marginalized  $1\sigma$  constraints on parameters with Reichart method.

model	sample	$\Omega_k$	$p_{\text{age}}$	$\eta$	$\gamma$	$\beta$	$\delta$
flat PAge	SNe+low-z QSOs	-	$1.05^{+0.051}_{-0.10}$	$0.140^{+0.36}_{-0.18}$	$0.750^{+0.013}_{-0.011}$	$3.72^{+0.32}_{-0.46}$	$0.244 \pm 0.0050$
	SNe+high-z QSOs	-	$0.919^{+0.033}_{-0.044}$	$0.570^{+0.16}_{-0.11}$	$0.681 \pm 0.016$	$5.84 \pm 0.51$	$0.213 \pm 0.0059$
non-flat PAge	SNe+low-z QSOs	$-0.240^{+0.12}_{-0.44}$	$1.20^{+0.29}_{-0.10}$	$-0.096^{+0.52}_{-0.39}$	$0.748^{+0.014}_{-0.012}$	$3.76^{+0.35}_{-0.44}$	$0.244 \pm 0.0050$
	SNe+high-z QSOs	$-0.638^{+0.081}_{-0.10}$	$1.26 \pm 0.11$	$-0.01^{+0.38}_{-0.26}$	$0.660 \pm 0.017$	$6.45 \pm 0.55$	$0.210 \pm 0.0058$

the fitting errors of the assumed background cosmology (Yang et al. 2020). According to the results shown in Figure 2, we confirm that the marginalized  $3\sigma$  constraints of SNe+QSOs on PAge parameters are in remarkable tension with the standard  $\Lambda$ CDM model in both flat and non-flat universes. This result agrees with Risaliti & Lusso (2019); Lusso et al. (2019, 2020).

We proceed to investigate the tension from the perspective of redshift evolution. By splitting QSOs into low-z and high-z samples, we find that there indeed exist remarkable discrepancies for the

slope  $\gamma$  parameter and intrinsic dispersion  $\delta$  between low-z and high-z QSOs calibrated by SNe. And the remarkable discrepancies for  $\gamma$  and  $\beta$  parameters persist in the parameter inferences derived from the Reichart method. These results reveal that the QSO luminosity correlation suffers from the redshift-evolution effect and non-universal intrinsic dispersion.

Building a QSO Hubble diagram with a non-robust QSO luminosity correlation may provide unreliable results. As indicated in Figure 3, with the evolutions of the  $\gamma$  and  $\delta$  parameters, the marginalized



contour of the SNe+low- $z$  QSOs sample is consistent with the  $\Lambda$ CDM while significant deviation emerges for the SNe+high- $z$  QSOs case. This indicates the PAge parameter constraints can be biased by the evolutions of  $\gamma$  and  $\delta$  parameters. Therefore, the significant deviation found in (Risaliti & Lusso 2019; Lusso et al. 2019, 2020) may mainly originate from the redshift-evolution effect and the non-universal intrinsic dispersion of the QSO luminosity correlation instead of new physics beyond the  $\Lambda$ CDM cosmology.

## ACKNOWLEDGEMENTS

We gratefully thank the authors in Lusso et al. (2020) for sharing the data used in this work. We thank Zhiqi Huang for the helpful discussions. This work is supported by the National Natural Science Foundation of China (NSFC) under Grant No. 12073088, National SKA Program of China No. 2020SKA0110402, National key R&D Program of China (Grant No. 2020YFC2201600), and Guangdong Major Project of Basic and Applied Basic Research (Grant No. 2019B030302001).

## 6 DATA AVAILABILITY

The quasar data underlying this article are available in Lusso et al. (2020) and in its online supplementary material. The supernova data underlying this article are publicly available in Scolnic et al. (2018).

## REFERENCES

Abbott T. M. C., et al., 2022, *Phys. Rev. D*, 105, 023520  
 Aghanim N., et al., 2020, *Astron. Astrophys.*, 641, A6  
 Alam S., et al., 2021, *Phys. Rev. D*, 103, 083533  
 Arcodia R., Merloni A., Nandra K., Ponti G., 2019, *A&A*, 628, A135  
 Baldwin J. A., 1977, *ApJ*, 214, 679  
 Bargiacchi G., Benetti M., Capozziello S., Lusso E., Risaliti G., Signorini M., 2022, *Mon. Not. Roy. Astron. Soc.*, 515, 1795  
 Bisogni S., Lusso E., Civano F., Nardini E., Risaliti G., Elvis M., Fabbiano G., 2021, *Astron. Astrophys.*, 655, A109  
 Cai R.-G., Guo Z.-K., Wang S.-J., Yu W.-W., Zhou Y., 2022a, *Phys. Rev. D*, 105, L021301  
 Cai R.-G., Guo Z.-K., Wang S.-J., Yu W.-W., Zhou Y., 2022b, *Phys. Rev. D*, 106, 063519  
 Colgáin E. O., Sheikh-Jabbari M. M., Solomon R., Bargiacchi G., Capozziello S., Dainotti M. G., Stojkovic D., 2022, *Phys. Rev. D*, 106, L041301  
 D'Agostini G., 2005  
 Ghisellini G., Haardt F., 1994, *Astrophys. J. Lett.*, 429, L53  
 Griffiths R. E., Maccacaro T., Murray S. S., Giacconi R., 1981, in *Andresen R. D., ed., X-Ray Astronomy*. Springer Netherlands, Dordrecht, pp 67–73  
 Guidorzi C., Frontera F., Montanari E., Rossi F., Amati L., Gomboc A., Mundell C. G., 2006, *Mon. Not. Roy. Astron. Soc.*, 371, 843  
 Haardt F., Maraschi L., 1991, *ApJ*, 380, L51  
 Haardt F., Maraschi L., 1993, *ApJ*, 413, 507  
 Huang Z., 2020, *Astrophys. J. Lett.*, 892, L28  
 Huang Z., 2022, *Commun. Theor. Phys.*, 74, 095404  
 Huang L., Huang Z., Li Z., Zhou H., 2021a, *Res. Astron. Astrophys.*, 21, 277  
 Huang L., Huang Z., Luo X., He X., Fang Y., 2021b, *Phys. Rev. D*, 103, 123521  
 Huang L., Huang Z., Zhou H., Li Z., 2022, *Sci. China Phys. Mech. Astron.*, 65, 239512  
 Jimenez R., Loeb A., 2002, *Astrophys. J.*, 573, 37  
 Khadka N., Ratra B., 2021, *Mon. Not. Roy. Astron. Soc.*, 502, 6140  
 Khadka N., Ratra B., 2022, *Mon. Not. Roy. Astron. Soc.*, 510, 2753  
 La Franca F., Bianchi S., Ponti G., Branchini E., Matt G., 2014, *Astrophys. J. Lett.*, 787, L12

Li X., Keeley R. E., Shafieloo A., Zheng X., Cao S., Biesiada M., Zhu Z.-H., 2021, *Mon. Not. Roy. Astron. Soc.*, 507, 919  
 Lian Y., Cao S., Biesiada M., Chen Y., Zhang Y., Guo W., 2021, *Mon. Not. Roy. Astron. Soc.*, 505, 2111  
 Luo X., Huang Z., Qian Q., Huang L., 2020, *Astrophys. J.*, 905, 53  
 Lusso E., 2019, *Astron. Nachr.*, 340, 267  
 Lusso E., Risaliti G., 2016, *ApJ*, 819, 154  
 Lusso E., Risaliti G., 2017, *A&A*, 602, A79  
 Lusso E., Piedipalumbo E., Risaliti G., Paolillo M., Bisogni S., Nardini E., Amati L., 2019, *Astron. Astrophys.*, 628, L4  
 Lusso E., et al., 2020, *Astron. Astrophys.*, 642, A150  
 Mehrabi A., Basilakos S., 2020, *Eur. Phys. J. C*, 80, 632  
 Melia F., 2019, *Mon. Not. Roy. Astron. Soc.*, 489, 517  
 Merloni A., 2003, *Mon. Not. Roy. Astron. Soc.*, 341, 1051  
 Nicastro F., 2000, *ApJ*, 530, L65  
 Perlmutter S., et al., 1997, *Bull. Am. Astron. Soc.*, 29, 1351  
 Perlmutter S., et al., 1999, *Astrophys. J.*, 517, 565  
 Reichart D. E., 2001, *ApJ*, 553, 235  
 Reichart D. E., Lamb D. Q., Fenimore E. E., Ramirez-Ruiz E., Cline T. L., Hurley K., 2001, *ApJ*, 552, 57  
 Riess A. G., et al., 1998, *Astron. J.*, 116, 1009  
 Risaliti G., Lusso E., 2015, *Astrophys. J.*, 815, 33  
 Risaliti G., Lusso E., 2019, *Nature Astron.*, 3, 272  
 Salvestrini F., Risaliti G., Bisogni S., Lusso E., Vignali C., 2019, *Astron. Astrophys.*, 631, A120  
 Schmidt B. P., et al., 1998, *Astrophys. J.*, 507, 46  
 Scolnic D. M., et al., 2018, *Astrophys. J.*, 859, 101  
 Tananbaum H., et al., 1979, *ApJ*, 234, L9  
 Tananbaum H., Avni Y., Green R. F., Schmidt M., Zamorani G., 1986, *ApJ*, 305, 57  
 Valcin D., Bernal J. L., Jimenez R., Verde L., Wandelt B. D., 2020, *JCAP*, 12, 002  
 Velten H., Gomes S., 2020, *Phys. Rev. D*, 101, 043502  
 Wang J.-M., et al., 2014, *Astrophys. J.*, 793, 108  
 Wang F., et al., 2021, *The Astrophysical Journal*, 907, L1  
 Watson D., Denney K. D., Vestergaard M., Davis T. M., 2011, *Astrophys. J. Lett.*, 740, L49  
 Yang T., Banerjee A., Colgáin E. O., 2020, *Phys. Rev. D*, 102, 123532  
 Yang J., et al., 2021, *Astrophys. J.*, 923, 262  
 Zheng X., Cao S., Biesiada M., Li X., Liu T., Liu Y., 2021, *Sci. China Phys. Mech. Astron.*, 64, 259511